

Multiple Myosins Are Required to Coordinate Actin Assembly with Coat Compression during Compensatory Endocytosis[□]

Hoi-Ying E. Yu* and William M. Bement*[†]

*Program in Cellular and Molecular Biology and [†]Department of Zoology, University of Wisconsin–Madison, Madison, WI 53706

Submitted November 8, 2006; Revised July 25, 2007; Accepted August 6, 2007
Monitoring Editor: David Drubin

Actin is involved in endocytosis in organisms ranging from yeast to mammals. In activated *Xenopus* eggs, exocytosing cortical granules (CGs) are surrounded by actin “coats,” which compress the exocytosing compartments, resulting in compensatory endocytosis. Here, we examined the roles of two myosins in actin coat compression. Myosin-2 is recruited to exocytosing CGs late in coat compression. Inhibition of myosin-2 slows coat compression without affecting actin assembly. This differs from phenotype induced by inhibition of actin assembly, where exocytosing CGs are trapped at the plasma membrane (PM) completely. Thus, coat compression is likely driven in part by actin assembly itself, but it requires myosin-2 for efficient completion. In contrast to myosin-2, the long-tailed myosin-1e is recruited to exocytosing CGs immediately after egg activation. Perturbation of myosin-1e results in partial actin coat assembly and induces CG collapse into the PM. Intriguingly, simultaneous inhibition of actin assembly and myosin-1e prevents CG collapse. Together, the results show that myosin-1e and myosin-2 are part of an intricate machinery that coordinates coat compression at exocytosing CGs.

INTRODUCTION

Actin assembly is associated with a variety of endocytic processes, including pinocytosis (Merrifield *et al.*, 1999), phagocytosis (May and Machesky, 2001), clathrin-mediated endocytosis (Merrifield *et al.*, 2004; Kaksonen *et al.*, 2005), and caveolae-mediated endocytosis (Pelkmans *et al.*, 2002). It has recently become apparent that actin assembly is also associated with regulated exocytosis in eggs (Becker and Hart, 1999; Sokac *et al.*, 2003), acinar cells (Nemoto *et al.*, 2004), and lung epithelial cells (van Weeren *et al.*, 2004). In these cell types, exocytosing secretory granules become surrounded with filamentous-actin (F-actin) coats, which can both stabilize the exocytotic compartment and promote the retrieval of its membrane in a form of compensatory endocytosis (for review, see Sokac and Bement, 2006). Although we know a considerable amount about the control and function of actin assembly in, for example, receptor-mediated endocytosis (Engqvist-Goldstein and Drubin, 2003; Merrifield *et al.*, 2004; Kaksonen *et al.*, 2005), we know relatively little

about the control of actin coats on exocytosing secretory granules.

Here, we have sought to better understand the mechanics of actin coat function in *Xenopus* eggs. In this system, cortical granules (CGs) undergo regulated exocytosis upon fertilization in response to elevated calcium. Shortly after CG fusion with the plasma membrane (PM), actin coats assemble around the exocytosing granules (Sokac *et al.*, 2003). Once the CG membrane surface has been completely surrounded by assembling actin, the actin coat compresses the CG membrane inward, thereby retrieving it (Sokac *et al.*, 2003). At least two processes have to be precisely coordinated for proper actin coat function. First, coats have to assemble on CGs only after CGs exocytose. If actin assembled before CG exocytosis, the coat might act as a barrier for exocytosis. Second, coat compression has to occur evenly on the exocytosing CGs. Otherwise, CG membrane might collapse into the PM, or be propelled around in the cytoplasm instead of being compressed.

Recently, we identified compartment-mixing as the mechanism that entrains actin coat assembly to exocytosis (Yu and Bement, 2007): when CGs exocytose, diacylglycerol from the PM incorporates into the CG membranes. Diacylglycerol, in turn, promotes protein kinase C β -dependent Cdc42 activation and coat assembly on the CG membrane (Yu and Bement, 2007). The assembled actin coat then works with myosin-1c, a short-tailed type 1 myosin, which couples the coat to the CG membrane during compression (Sokac *et al.*, 2006).

How, exactly, does coat compression work and what players ensure that it works properly? One possibility is that compression is driven by actin assembly itself (Sokac *et al.*, 2003, 2006). It is also possible that other myosins, in addition to myosin-1c, participate in the compression. For example, myosin-2 is well known to associate with actin to drive

This article was published online ahead of print in *MBC in Press* (<http://www.molbiolcell.org/cgi/doi/10.1091/mbc.E06-11-0993>) on August 15, 2007.

[□] The online version of this article contains supplemental material at *MBC Online* (<http://www.molbiolcell.org>).

Address correspondence to: Hoi-Ying E. Yu (heyu@uwalumni.com).

Abbreviations used: 4D, time-lapse multiple focal plane; CG, cortical granule; eGFP, enhanced green fluorescent protein; F-actin, filamentous actin; G-actin, globular actin; IP₃, inositol-1,4,5-trisphosphate; mRFP, monomeric red fluorescent protein; MyTH, myosin tail homology; PM, plasma membrane; rGBD, RhoA-binding domain of rhotekin; SH3, src homology 3; TR, Texas red; Utr₁₋₂₆₁, F-actin binding domain of utrophin.

contraction (Matsumura, 2005), and long-tailed type 1 myosins have been shown to play key roles in actin-mediated endocytosis in yeast (Sirotkin *et al.*, 2005; Sun *et al.*, 2006). As described below, we find evidence for participation of these myosins, as well as actin assembly itself, in compression of actin coats.

MATERIALS AND METHODS

Preparation of Probes

Utr₁₋₂₆₁-mRFP and Utr₁₋₂₆₁-eGFP, provided by B. Burkel (University of Wisconsin–Madison), are monomeric red fluorescent protein (mRFP) and enhanced green fluorescent protein (eGFP) fused with amino acid 1-261 of utrophin, which corresponds to the calponin homology domain and binds to F-actin (Burkel *et al.*, 2007). Rhodamine myosin-2 (provided by J. Pelouquin, University of Wisconsin–Madison) was prepared from turkey gizzards and labeled with tetramethylrhodamine maleimide (Verkhovskiy *et al.*, 1995). Farnesylated-eGFP was provided by M. V. Danilchik (Oregon Health and Science University, Portland, OR). *Xenopus laevis* myosin-1e (accession no. BC046842) was cloned from cDNA obtained from stage 4 oocytes.

All subclonings were done by polymerase chain reaction (PCR). Full-length or truncated myosin-1e was cloned into custom pCS2 vector, pCS2-eGFP vector (Sokac *et al.*, 2003) or pCS2-mRFP vector (mRFP cDNA provided by R. Tsen, University of California–San Diego, La Jolla, CA) and subsequently cloned into pCS2 vector. Full-length or truncated myosin-1e was cloned downstream of the eGFP or mRFP. Myosin tail homology (MyTH2) was cloned downstream of the glutathione S-transferase (GST) in the pGEX vector (GE Healthcare, Little Chalfont, Buckinghamshire, United Kingdom). GST-MyTH2 was then subcloned into pCS2 vector. All probes were transcribed *in vitro* by using the SP6 mMessage mMachine kit (Ambion, Austin, TX) for microinjection into oocytes.

Egg Procurement and Microinjection

Oocytes were obtained from adult *Xenopus* females, defolliculated, and stored in Barth's solution (87.4 mM NaCl, 1 mM KCl, 2.4 mM NaHCO₃, 0.82 mM MgSO₄, 0.6 mM NaNO₃, 0.7 mM CaCl₂, and 10 mM HEPES, pH 7.4), with 0.1 mg/ml gentamicin and 6 µg/ml tetracycline. Microinjections were performed using a PLI-100 picoinjector (Medical Systems, Greenvale, NY), and for oocytes requiring multiple microinjections, there was a minimum of 1-h recovery time between consecutive microinjections.

For wound healing experiments, protein probes were injected to final intracellular concentrations as follows: 20 µg/ml Alexa488 globular-actin (G-actin) (Invitrogen, Carlsbad, CA) and 20 µg/ml Alexa568 G-actin (Invitrogen); and capped mRNAs were injected to final intracellular concentrations as follows: 40 µg/ml Utr₁₋₂₆₁-mRFP, 20 µg/ml Utr₁₋₂₆₁-eGFP, 40 µg/ml eGFP-myosin-1e, and 128 µg/ml mRFP-MyTH2 (of myosin-1e). For the F-actin cosedimentation assay, capped mRNA was injected to final intracellular concentrations as follows: 80 µg/ml GST and 80 or 160 µg/ml GST-MyTH2. For CG exocytosis experiments, proteins or chemicals were injected to attain final intracellular concentrations as follows: 10 µM photolyze nitrophenylethyl ester (NPE)-caged inositol 1,4,5-trisphosphate (IP₃) (Invitrogen), 80 µg/ml Alexa488 G-actin (Invitrogen), and 400 µg/ml rhodamine myosin-2; and capped mRNA were injected to final intracellular concentrations as follows: 4 µg/ml farnesylated-eGFP, 40 µg/ml RhoA-binding domain of rhotekin (rGBD)-eGFP, 40 µg/ml Utr₁₋₂₆₁-mRFP, 24 µg/ml untagged full-length myosin-1e, 24 µg/ml untagged headless myosin-1e, 54 µg/ml eGFP-myosin-1e, 80 µg/ml eGFP-myosin-1e ΔSH3, 32 µg/ml eGFP-headless myosin-1e, 40 µg/ml eGFP-headless myosin-1e ΔSH3, 40 µg/ml eGFP-MyTH1-MyTH2-SH3 (of myosin-1e), 140 µg/ml eGFP-MyTH1-MyTH2 (of myosin-1e), 120 µg/ml eGFP-head (of myosin-1e), 80 µg/ml eGFP-head-IQ (of myosin-1e), 160 µg/ml eGFP-SH3 (of myosin-1e), 160 µg/ml eGFP-Head-IQ-MyTH1 (of myosin-1e), 160 µg/ml eGFP-IQ (of myosin-1e), 240 µg/ml eGFP-MyTH1 (of myosin-1e), 56 µg/ml eGFP-MyTH2 (of myosin-1e), 240 µg/ml eGFP-myosin-1e-ΔMyTH1, and 128 µg/ml mRFP-MyTH2 (of myosin-1e). When higher concentration of headless myosin-1e was used, CG exocytosis was often inhibited (data not shown). For CG exocytosis experiments, all microinjections were done at least 4 h before induction of meiotic maturation, which was triggered by incubating oocytes in Barth's solution containing 5 µg/ml progesterone for 8–14 h to obtain eggs.

F-Actin Cosedimentation Experiment

After microinjection with capped mRNA encoding either GST or GST-MyTH2, oocytes were incubated overnight to allow for expression. Cells were homogenized with buffer containing 50 mM KCl, 1 mM EGTA, 20 mM piperazine-*N,N'*-bis(2-ethanesulfonic acid), pH 7.0, 1 mM MgCl₂, protease inhibitors, and 1 µM phalloidin at 4°C. To disassemble the F-actin, a parallel experiment was done where oocytes microinjected with either GST or GST-MyTH2 were treated with 5 µM latrunculin (Calbiochem, San Diego, CA) for 1 h before homogenization. Oocytes were then homogenized as described

above, but with 5 µM latrunculin and no phalloidin. The homogenates were centrifuged at 5000 × *g* for 5 min at 4°C to pellet yolk. The supernatants were then subsequently centrifuged in an airfuge at 20 psi (100,000 × *g*) for half an hour at 4°C. Equal amounts of supernatant and pellet were separated on a SDS-polyacrylamide gel electrophoresis, and transferred to nitrocellulose. Immunoblotting was performed using primary anti-GST antibody (GE Healthcare), and secondary anti-goat coupled to horseradish peroxidase-conjugated antibody (Promega, Madison, WI). Blots were developed using ECL Western blotting substrate (Pierce Chemical, Rockford, IL).

Cell Manipulation and Live Imaging

Single-plane, time-lapse imaging of CG exocytosis was performed using a Zeiss Axiovert 100 M microscope (Carl Zeiss, Thornwood, NY) with Bio-Rad Lasersharp Confocal software (Bio-Rad, Hercules, CA) similar to that described previously (Sokac *et al.*, 2003). Eggs were mounted and imaged with either 3000 mol. wt. neutral Texas Red (TR)-dextran or 10,000 mol. wt. Alexa647 dextran (Invitrogen) to allow visualization of exocytosing CGs. While imaging, egg activation was triggered by focusing UV light onto the egg cortex for 3–5 s to photolyze NPE-caged IP₃ (Invitrogen). In experiments where cytochalasin D (Calbiochem) was used, cells were mounted in the presence of TR-dextran containing a final concentration of 5 µM cytochalasin D for 4 min before activation. Increased doses of cytochalasin D resulted in collapse of exocytosing CG membrane into the PM, similar to that induced by 30-min treatment of latrunculin (data not shown). In experiments where blebbistatin (Calbiochem) was used, cells were incubated with either 200 µM (±)-blebbistatin or inactive (+)-blebbistatin in Barth's solution containing progesterone at the time when meiotic maturation was induced.

Time-lapse multiple focal plane (4D) imaging on wound healing was performed as described previously (Mandato and Bement, 2001). Laser wounds were made with a Micropoint pulse nitrogen-pumped dye laser (Laser Science, Franklin, MA). Actin comet formation was stimulated by incubating cells in deuterium oxide (Sigma-Aldrich, St. Louis, MO) to up-regulate microtubules, a manipulation that promotes comet assembly (Mandato and Bement, 2003). Movies were generated with Velocity 3.1 software (Improvision, Lexington, MA). Montages were subsequently made with Adobe Photoshop 7.0 (Adobe Systems, Mountain View, CA).

Data Quantification and Statistical Analysis

Object-Image 2.10 software or ImageJ 1.34s (Both from National Institutes of Health, Bethesda, MD) was used to measure fluorescence intensities as described previously (Yu and Bement, 2007), as well as band intensity in immunoblots. CG membrane retrieval time was measured by determining the time during which the dextran-filled compartments existed. Statistical analysis was performed using Excel (Microsoft, Redmond, WA). Two-tailed Student's *t* test was used to compare whether there was significant differences between two sets of data when appropriate.

RESULTS

Exocytosing CG Compartments Are Not Retrieved in Cytochalasin D-treated Eggs

Although F-actin has been shown to be crucial in retrieving the exocytosing CG membrane (Sokac *et al.*, 2003), the role played by actin assembly is not clear. One possibility is that assembling actin compresses coats (Sokac *et al.*, 2006). If this idea is correct, then a brief treatment with cytochalasin D, which inhibits actin assembly by binding to the barbed end of the actin filament, should limit coat formation. Exocytosis was triggered in the presence of TR-dextran, which filled the CG compartments upon exocytosis and showed up as red discs (Figure 1A; Sokac *et al.*, 2003). In control cells, actin coats assembled on CGs after exocytosis and then compressed, retrieving the CG compartments within ~50 s (Figure 1A; Sokac *et al.*, 2003). In contrast, when cells were treated with cytochalasin D, actin coats failed to assemble on most exocytosing CGs (Figure 1A), and exocytosed CGs remained trapped under the PM as discrete compartments for 5 min or more (Figure 1). Because nearly all exocytosed CGs remained intact at the end of the imaging series of 4–5 min, the time of retrieval shown in Figure 1C represents a significant underestimation. Thus, exocytosing CGs cannot be retrieved in the absence of actin coats. Actin coats occasionally occurred around a few exocytosing CGs in cytochalasin D-treated cells; however, these coats failed to compress

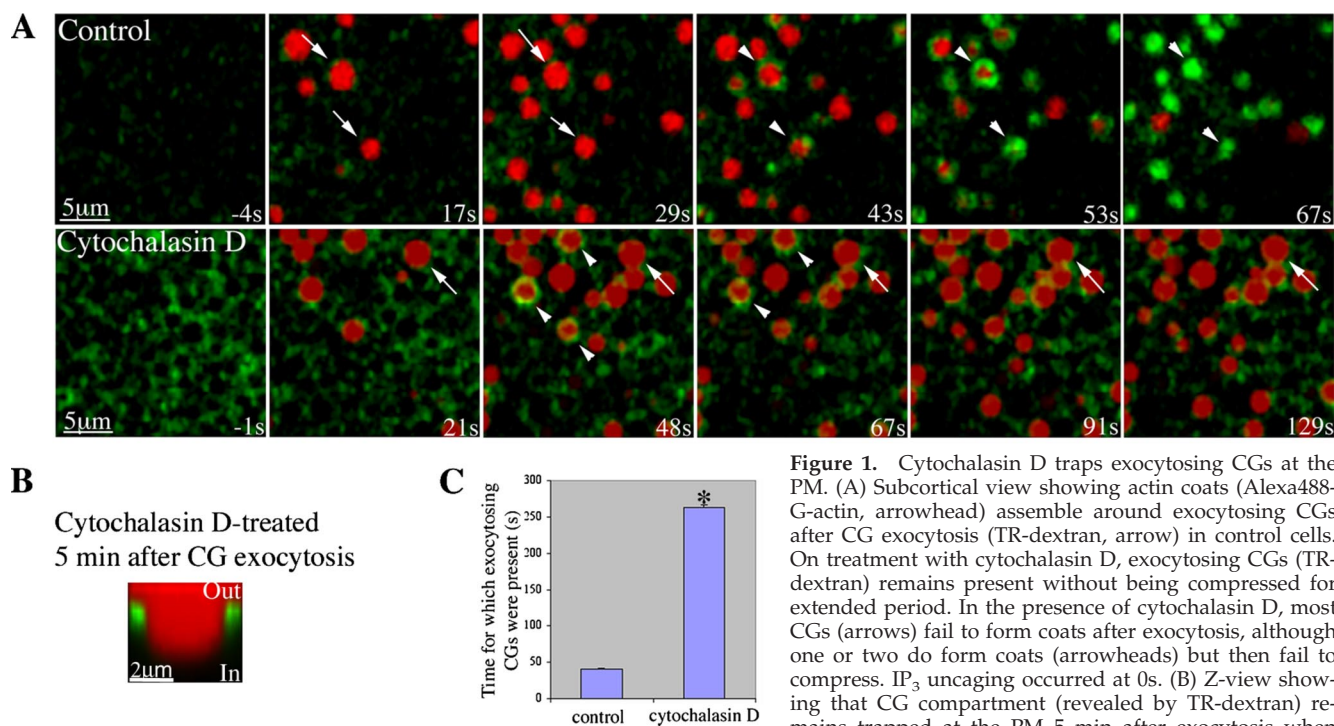


Figure 1. Cytochalasin D traps exocytosing CGs at the PM. (A) Subcortical view showing actin coats (Alexa488-G-actin, arrowhead) assemble around exocytosing CGs after CG exocytosis (TR-dextran, arrow) in control cells. On treatment with cytochalasin D, exocytosing CGs (TR-dextran) remains present without being compressed for extended period. In the presence of cytochalasin D, most CGs (arrows) fail to form coats after exocytosis, although one or two do form coats (arrowheads) but then fail to compress. IP₃ uncaging occurred at 0s. (B) Z-view showing that CG compartment (revealed by TR-dextran) remains trapped at the PM 5 min after exocytosis when treated with cytochalasin D. (C) Quantification of time for

which the exocytosing CGs are present ($n = 84$ for control, $n = 69$ for cytochalasin D treated; asterisk indicates a $p = 1 \times 10^{-114}$; error bar is SEM). For control, the time represents the average time taken to retrieve the exocytosing CG membrane. For cytochalasin D-treated cells, the time represents a significant underestimation because most CGs are still present after 4.5 min.

(Figure 1A). The observation that cytochalasin D, which blocks barbed end actin assembly, prevents coat compression even when actin is present (Figure 1A), is consistent with the possibility that plus-end actin assembly is responsible for compressing the CGs under normal circumstances. However, it is also possible that the actin coats that form in the presence of cytochalasin cannot interact properly with myosins and thus fail to compress.

Myosin-2 Is Required for Efficient Actin Coat Compression

To test the potential role of myosin-2 in coat compression, we used rhodamine-labeled smooth muscle myosin-2. This probe has previously been shown to colocalize with *Xenopus* myosin-2A in fixed *Xenopus* oocytes (Mandato and Bement, 2001) and to serve as a faithful mimic of nonmuscle myosin-2A distribution and dynamics in living cultured cells (Kolega, 1998). Because nonmuscle myosin-2A comprises >95% of the myosin-2 in *Xenopus* eggs (Kelley *et al.*, 1996), we consider rhodamine-labeled smooth muscle myosin-2 a reasonable surrogate for myosin-2A in this system, although we cannot rule out the possibility that it does not completely mimic myosin-2A dynamics in eggs. After uncaging of IP₃, rhodamine-labeled smooth muscle myosin-2 was recruited to exocytosing CGs, with the onset of recruitment occurring after CG compression had begun (Figure 2, A and D, and Supplemental Figure 1). Simultaneous imaging of myosin-2 and actin during CG membrane retrieval revealed that myosin-2 recruitment occurred ~13 s after actin recruitment (Figure 2, B and D, and Supplemental Figure 1).

To further test the role of myosin-2 during CG membrane retrieval, we treated the eggs with (\pm)-blebbistatin to inhibit myosin-2 activity (Straight *et al.*, 2003). Due to photoinacti-

vation of (\pm)-blebbistatin by wavelengths that excite eGFP (Kolega, 2004), CG membrane retrieval and actin coat assembly were monitored separately using red fluorescent probes. Treatment of (\pm)-blebbistatin increased the time taken to retrieve exocytosing CG membrane compared with cells treated with the inactive (+)-enantiomer of blebbistatin (Figure 2, E and E'). In addition, (\pm)-blebbistatin prolonged the presence of actin coats without affecting actin coat assembly (Figure 2, F and F'). Interestingly, coat compression and membrane retrieval was ultimately achieved when treated with (\pm)-blebbistatin (Figure 2, E and F) in contrast to what was observed upon treatment with cytochalasin D. Together, our results imply that myosin-2 does not drive coat compression but that it is required for efficient completion of coat compression.

Because RhoA is a common upstream activator of myosin-2 (Kimura *et al.*, 1996), we determined whether RhoA was activated during CG membrane retrieval. eGFP-rGBD (Benink and Bement, 2005) was used to monitor RhoA activity. RhoA was activated around the exocytosing CGs ~3 s before actin coat assembly (Figure 2, C and D, and Supplemental Figure 1). To further elucidate the relative time of RhoA activation and myosin-2 recruitment, we compared their recruitment times to actin assembly. This confirmed that RhoA was activated before actin assembly, which was followed by the beginning of coat compression, and then myosin-2 recruitment (Figure 2D and Supplemental Figure 1), consistent with the possibility that myosin-2 recruitment depends on RhoA activation.

Myosin-1e Is Recruited to Exocytosing CGs

Long-tailed type 1 myosins are involved in endocytosis in yeast (Sirotkin *et al.*, 2005; Sun *et al.*, 2006), and they can bind

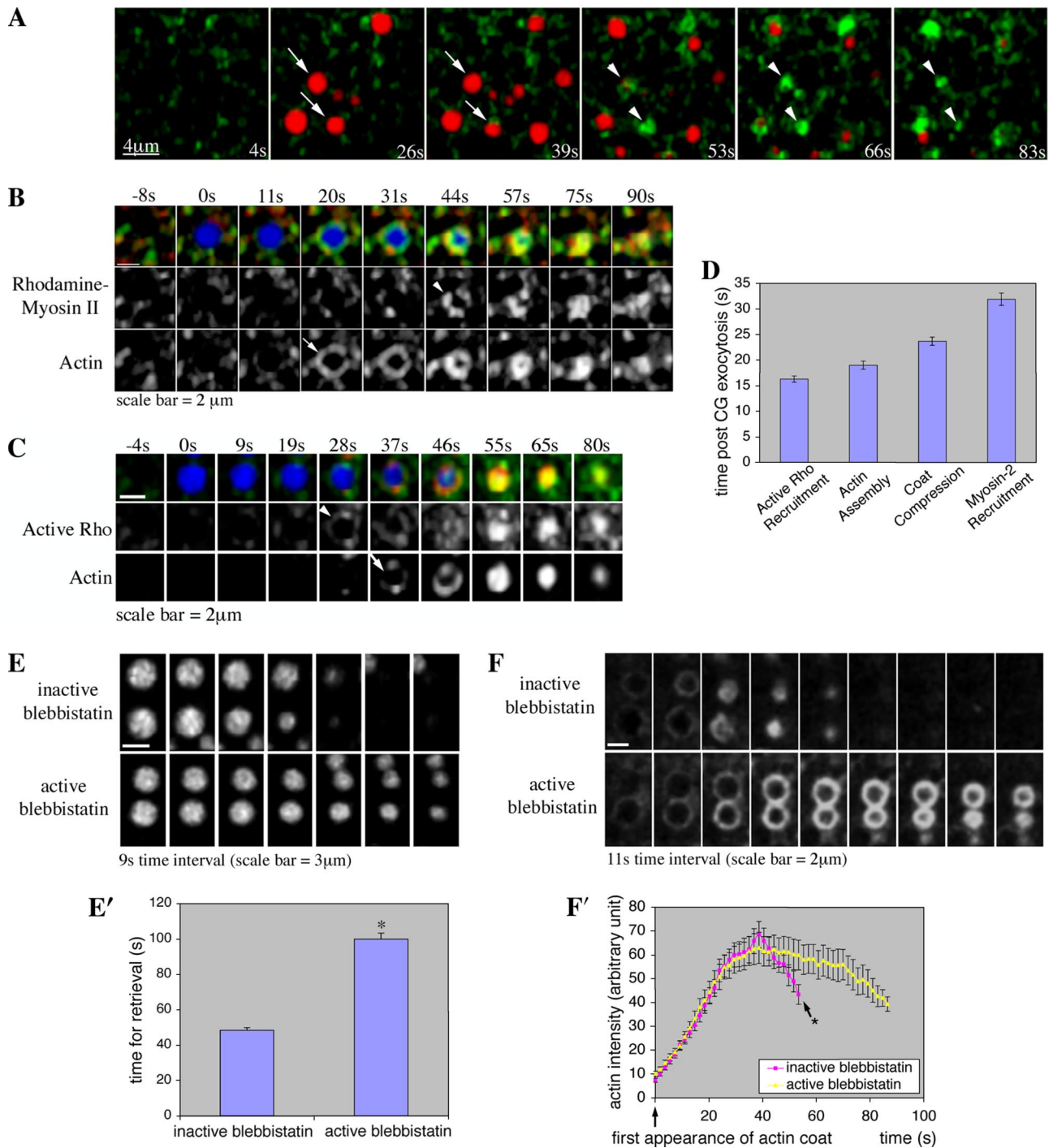


Figure 2. Myosin-2 is required for efficient coat compression. (A) Subcortical view showing myosin-2 (rhodamine myosin-2, pseudocolored in green, arrowhead) is recruited to exocytosing CGs (Alexa647 dextran, pseudocolored in red, arrow) after onset of coat compression. IP₃ uncaging occurred at 0s. (B) Subcortical view showing simultaneous imaging of myosin-2 and actin recruitment to CG in the presence of Alexa647 dextran (blue). Myosin-2 (rhodamine myosin-2, red, arrowhead) is recruited to exocytosing CGs (Alexa647 dextran) after actin coat (Alexa488 G-actin, green, arrow) is assembled. 0s indicates time at which CG exocytoses. (C) Subcortical view showing simultaneous imaging of active RhoA and actin recruitment to CG in the presence of Alexa647 dextran (blue). RhoA is activated (rGBD-eGFP, green, arrowhead) at the exocytosing CGs (Alexa647 dextran) just before the onset of actin coat (Utr₁₋₂₆₁-mRFP, red, arrow) assembly. 0s indicates the time at which CG exocytoses. (D) Time at which myosin-2 and active RhoA are recruited to CGs with respect to the onset of actin assembly and coat compression (all of which are statistically different from one another with $p < 0.001$). (E) Subcortical view showing exocytosing CGs (TR-dextran) take longer to be retrieved when treated with active blebbistatin. The first frame indicates the time at which CGs first exocytosed. (E') Quantification of time taken to retrieve CG membrane [$n = 68$ for inactive (+)-blebbistatin, $n = 70$ for active (\pm)-blebbistatin; error bar is SEM; asterisk indicates a $p = 1 \times 10^{-27}$]. (F) Subcortical view showing that active (\pm)-blebbistatin prolongs the presence of actin coats, without affecting the rate of actin coat (Utr₁₋₂₆₁-mRFP) assembly compared with inactive (+)-blebbistatin-treated cells. The first frame indicates the first appearance of actin coat. (F') Quantification of the intensity of actin coats at exocytosing CGs ($n = 29$ for each group). No data are available for time points after that noted with asterisk, because CG membrane is retrieved by then (see E and E'); consequently, there is no longer any actin coat (see F).

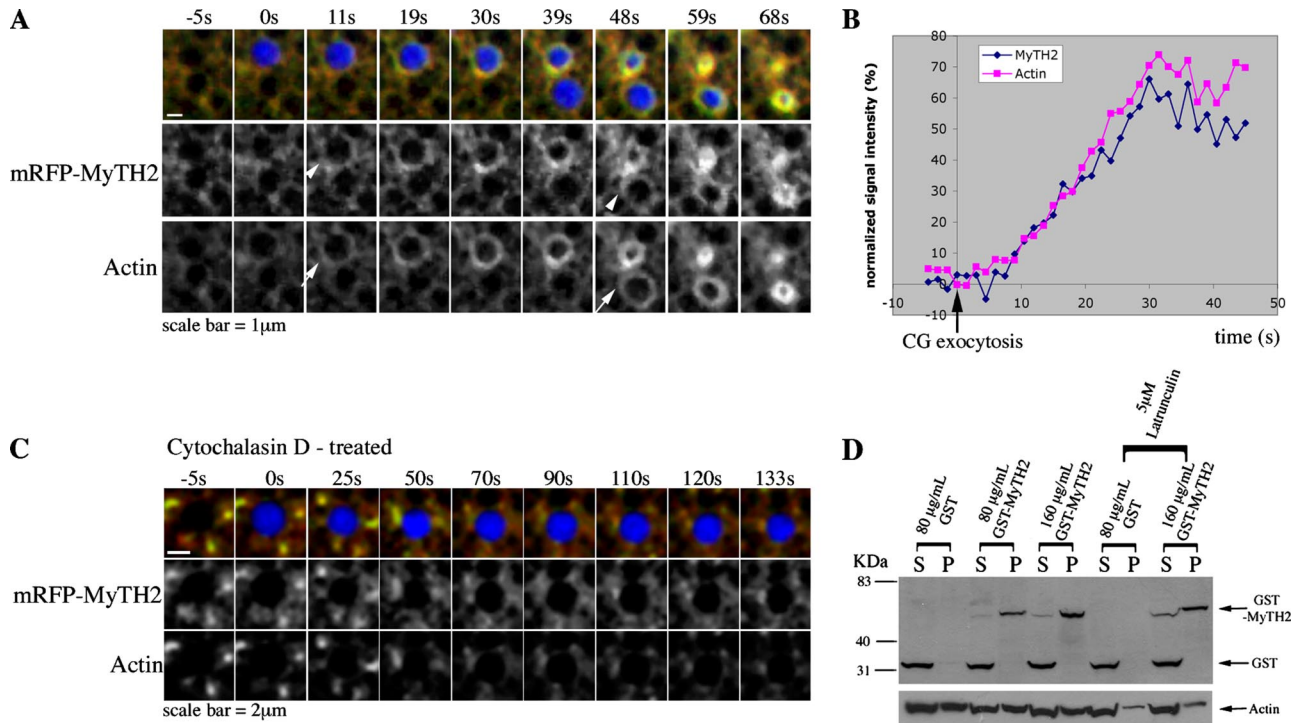


Figure 4. MyTH2 recruitment to CGs depends on actin coat assembly. (A) Subcortical images showing that mRFP-MyTH2 (red, arrowhead) is recruited to the exocytosing CGs (Alexa647 dextran, blue) at about the same time as the onset of actin coat (Alexa488 G-actin, green, arrow) assembly. 0s indicates the time at which CG exocytoses. (B) Quantification of the intensity of MyTH2 and actin coats on CGs ($n = 10$). (C) Subcortical images showing that inhibition of actin coat (Alexa488 G-actin, green) assembly by cytochalasin D also prevents mRFP-MyTH2 (red) recruitment to exocytosing CGs (Alexa647 dextran, blue). 0s indicates the time at which CG exocytoses. (D) F-actin cosedimentation assay showing that MyTH2 associates with F-actin. Oocytes microinjected with the indicated final concentration of GST or GST-MyTH2 RNA, with or without pretreatment of latrunculin, are homogenized and ultracentrifuged to pellet the F-actin. GST was present in cells injected with RNA encoding GST-MyTH2, probably due to proteolysis of the GST-MyTH2 construct. P, pellet; S, supernatant.

1e- Δ MyTH1) were only recruited to CGs after exocytosis and were not present on the PM (Figure 3, G and H; see below). Thus, MyTH1 is essential for the initial CG recruitment and the PM localization of myosin-1e. Finally, constructs that lacked the MyTH2 domain (eGFP-head, eGFP-head-IQ, eGFP-IQ, eGFP-SH3, and eGFP-MyTH1) did not localize to CGs or the PM (Figure 3, F and H). Together, these data show that MyTH1 and MyTH2 are the minimal domains required for proper recruitment of myosin-1e to the CGs (Figure 3, D and H).

MyTH2 Is Associated with More Dynamic F-Actin

As mentioned above, MyTH2 was recruited to CGs only after exocytosis, whereas full length myosin-1e was recruited to CGs before exocytosis. Because MyTH2 binds F-actin in protozoa (Doberstein and Pollard, 1992; Jung and Hammer, 1994), we compared the recruitment of MyTH2 with actin assembly. Simultaneous imaging of the recruitment of both actin and MyTH2 revealed that MyTH2 was recruited to CGs at about the same time as the onset of actin coat assembly (Figure 4A). Furthermore, quantification of MyTH2 and actin signal intensity showed that MyTH2 recruitment to CGs increased at about the same rate as actin (Figure 4B), consistent with the possibility that MyTH2 recruitment was dependent on actin coat assembly. In addition, when cells were treated with cytochalasin to block actin assembly, MyTH2 was no longer recruited to the CGs (Figure 4C), further suggesting that this domain is targeted by virtue of its interaction with F-actin. As an additional means to determine whether MyTH2 can bind to F-actin, we

determined whether MyTH2 can cosediment with F-actin upon ultracentrifugation. Cells expressing GST, or different concentrations of GST-MyTH2, were homogenized and subjected to ultracentrifugation to separate the G-actin and F-actin. Although GST was present in the soluble fraction along with the G-actin, GST-MyTH2 was present in the pellet fraction with the F-actin (Figure 4D). If MyTH2 is indeed associated with F-actin, disassembly of F-actin should reduce the amount of both the actin and MyTH2 in the pellet. Cells were treated with latrunculin for 1 h before homogenization to reduce the amount of F-actin in cells. After treatment with latrunculin, 58% less actin and 23% less GST-MyTH2 was pelleted (Figure 4D). These results further support the notion that MyTH2 associates with F-actin *in vivo*.

Because the aforementioned results indicated that the myosin-1e MyTH2 domain associates with F-actin, and because actin coats are made up of highly dynamic actin (Sokac *et al.*, 2003), we sought to determine whether MyTH2 might preferentially associate with dynamic actin. To accomplish this, we examined the recruitment of MyTH2 around *Xenopus* oocyte wounds that are characterized by a region of stable actin near the wound edge, and a region of highly dynamic actin $\sim 5 \mu\text{m}$ away from the wound edge (Mandato and Bement, 2001, 2003; Burkel *et al.*, 2007). Fluorescent G-actin labels the region of highly dynamic F-actin relatively better than either fluorescent phalloidin (Mandato and Bement, 2001, 2003) or fluorescent versions of the Utr₁₋₂₆₁ (Figure 5, A and A'; Burkel *et al.*, 2007). Comparison of RFP-MyTH2 with GFP-Utr₁₋₂₆₁ showed that the MyTH2 domain preferentially

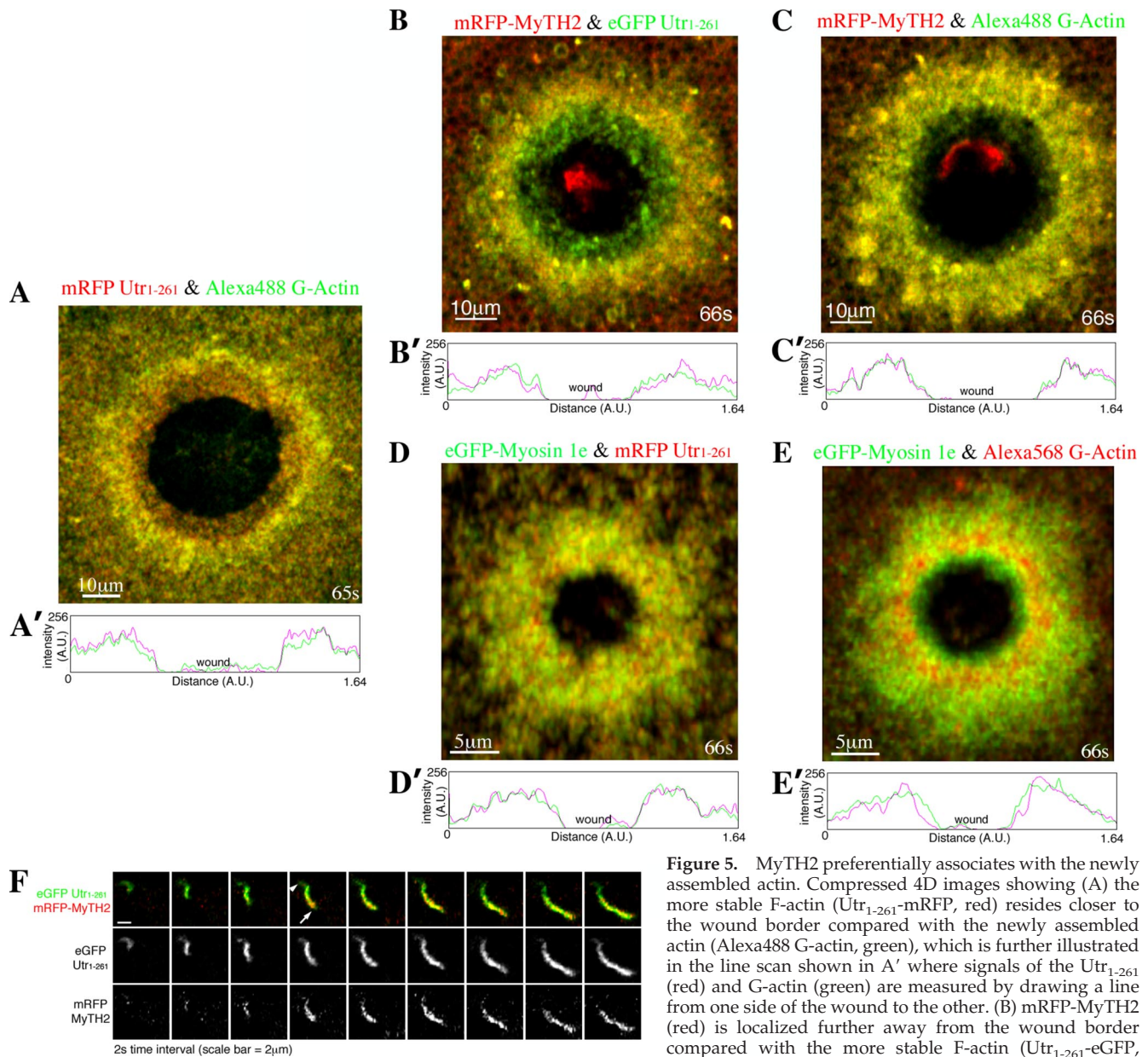


Figure 5. MyTH2 preferentially associates with the newly assembled actin. Compressed 4D images showing (A) the more stable F-actin (Utr₁₋₂₆₁-mRFP, red) resides closer to the wound border compared with the newly assembled actin (Alexa488 G-actin, green), which is further illustrated in the line scan shown in A' where signals of the Utr₁₋₂₆₁ (red) and G-actin (green) are measured by drawing a line from one side of the wound to the other. (B) mRFP-MyTH2 (red) is localized further away from the wound border compared with the more stable F-actin (Utr₁₋₂₆₁-eGFP, green), which is further illustrated in the line scan shown in B' where signals of the Utr₁₋₂₆₁ (green) and MyTH2 (red) are measured by drawing a line from one side of the wound to the other. (C) mRFP-MyTH2 (red) colocalizes with the newly assembled actin (Alexa488 G-actin, green) around the oocyte wound; which is further illustrated in the line scan shown in C' where signals of the G-actin (green) and MyTH2 (red) are measured by drawing a line from one side of the wound to the other. (D) eGFP-myosin-1e (green) localizes with the stable F-actin (Utr₁₋₂₆₁-mRFP, red) around the oocyte wound, which is further illustrated in the line scan shown in D' where signals of the Utr₁₋₂₆₁ (red) and myosin-1e (green) are measured by drawing a line from one side of the wound to the other. (E) eGFP-myosin-1e (green) localizes with the newly assembled actin (Alexa568 G-actin, red) around the oocyte wound, which is further illustrated in the line scan shown in E' where signals of the myosin-1e (green) and G-actin (red) are measured by drawing a line from one side of the wound to the other. Oocytes are wounded at 0s in A–E. (F) Images showing the assembly of a newly polymerized actin comet, where mRFP-MyTH2 (red) and Utr₁₋₂₆₁-eGFP (green) are present. Notice that mRFP-MyTH2 (red) is more prominent at the head (arrow), rather than the tail (arrowhead) of the actin comet.

in (B') where signals of the Utr₁₋₂₆₁ (green) and MyTH2 (red) are measured by drawing a line from one side of the wound to the other. (C) mRFP-MyTH2 (red) colocalizes with the newly assembled actin (Alexa488 G-actin, green) around the oocyte wound; which is further illustrated in the line scan shown in C' where signals of the G-actin (green) and MyTH2 (red) are measured by drawing a line from one side of the wound to the other. (D) eGFP-myosin-1e (green) localizes with the stable F-actin (Utr₁₋₂₆₁-mRFP, red) around the oocyte wound, which is further illustrated in the line scan shown in D' where signals of the Utr₁₋₂₆₁ (red) and myosin-1e (green) are measured by drawing a line from one side of the wound to the other. (E) eGFP-myosin-1e (green) localizes with the newly assembled actin (Alexa568 G-actin, red) around the oocyte wound, which is further illustrated in the line scan shown in E' where signals of the myosin-1e (green) and G-actin (red) are measured by drawing a line from one side of the wound to the other. Oocytes are wounded at 0s in A–E. (F) Images showing the assembly of a newly polymerized actin comet, where mRFP-MyTH2 (red) and Utr₁₋₂₆₁-eGFP (green) are present. Notice that mRFP-MyTH2 (red) is more prominent at the head (arrow), rather than the tail (arrowhead) of the actin comet.

concentrated with the region of dynamic actin, well back from the wound edge (Figure 5, B and B'). Indeed, mRFP-MyTH2 colocalized with Alexa488 G-actin (Figure 5, C and C'), our marker for dynamic actin. The full-length myosin-1e, in contrast, was found in the regions of both the stable and the dynamic actin, as judged by comparison of GFP-myosin-1e with either mRFP-Utr₁₋₂₆₁ (Figure 5, D and D') or Alexa568 G-actin (Figure 5, E and E').

As an additional test of the idea that the MyTH2 domain of myosin-1e preferentially associates with dynamic F-actin, we followed the distribution of mRFP-MyTH2 and GFP-Utr₁₋₂₆₁ in actin comets, which form in response to wounding (Mandato and Bement, 2001). Because the actin assembles at the head of the comet, the newest filaments are located there, whereas the filaments in the tail of the comet are older. Although both mRFP-MyTH2 and GFP-Utr₁₋₂₆₁ were found at the comet, the

mRFP-MyTH2 was relatively more concentrated near the heads of comets (Figure 5F), consistent with the idea that it associates with rapidly assembling F-actin.

Myosin-1e Ensures Symmetric Coat Assembly and Prevents CG Membrane Collapse

We next sought to determine what contributions, if any, myosin-1e makes to coat function. To accomplish this, we expressed a headless myosin-1e (a construct that lacks the motor domain) to see whether coat compression was impeded. As shown in Figure 3, A–H, this construct is recruited with normal kinetics to CGs after IP₃ uncaging, and headless constructs have long been used as dominant negatives to inhibit specific isoform of myosins (Durrbach *et al.*, 1996; Rogers *et al.*, 1999; Bose *et al.*, 2002; Sokac *et al.*, 2006). To ensure that the levels of headless myosin-1e did not inhibit CG exocytosis (Schietroma *et al.*, 2007), the amount of injected mRNA was carefully titrated (see *Materials and Methods*).

Because myosin-1e is a motor, and because it localizes to exocytosing CGs, we anticipated that the headless construct would slow coat compression and delay disappearance of the dextran marker in exocytosing CGs. Surprisingly, however, we found that the headless myosin-1e resulted in faster disappearance of the dextran marker (Figure 6, A and D). To confirm the specificity of this phenotype, we expressed both the headless construct and full-length myosin-1e. This partially rescued the phenotype seen with the headless construct alone (Figure 6, A and D), indicating that the headless construct is working by displacing the endogenous full-length myosin-1e.

To better understand how headless myosin-1e induces faster loss of the dextran marker, actin coat assembly was monitored in eggs expressing the headless myosin-1e construct. Quantification of actin coat assembly in the presence of headless myosin-1e revealed that coats were relatively normal until ~30 s after CG exocytosis (Figure 6C). However, because the dextran loss was observed in headless myosin-1e-expressing cells immediately after exocytosis, this deficit is unlikely to account for the phenotype.

We next monitored actin assembly and membrane retrieval simultaneously in *z* movies. In contrast to controls (Figure 6B), wherein the assembling actin could be clearly seen to encircle the entire exocytosing CG, in cells expressing headless myosin-1e, the actin failed to completely enclose the exocytosing CG and instead concentrated on the basal portion of the exocytosing CG (Figure 6B).

These findings suggested that the abnormally rapid loss of the dextran-containing compartments might reflect asymmetric compression of the coats commencing from the basal side of the compartment and moving upward, thereby rapidly expelling the dextran and causing the collapse of the CG membrane into the PM and failure of proper CG membrane retrieval. To test this idea, cells expressing headless myosin-1e were treated with low doses of cytochalasin, to prevent actin assembly, coat formation, and coat compression (Figure 1). Low doses of cytochalasin suppressed the rapid loss of dextran caused by the headless myosin-1e (Figure 6, E and F). This is consistent with the idea that the asymmetric actin coat in the headless myosin-1e cells induces CG membrane collapse and hence rapid loss of dextran. Collectively, the results indicated that myosin-1e helps resist coat compression and may also prevent the actin that forms the coat from accumulating in an asymmetric manner.

DISCUSSION

The results of this study reveal the existence of a precisely orchestrated machinery that is required to drive coat com-

pression after CG exocytosis in *Xenopus* eggs. Our findings suggest that plus-end actin polymerization and myosin-2 are required to compress the exocytosing compartments, whereas myosin-1e is required to stabilize the exocytosing CGs at the PM by preventing premature coat compression. As detailed below, the distinct functions and recruitment patterns of these and other proteins lead to a model wherein different myosins cooperate with cortical actin and actin coats to drive CG membrane retrieval.

Although brief perturbation of actin assembly by cytochalasin D trapped exocytosing CGs at the PM without collapsing into the PM (this study), disruption of actin by a half-hour latrunculin treatment induces rapid collapse of CG membrane into the PM after exocytosis (Sokac *et al.*, 2003). How does disruption of actin in these two cases lead to different phenotypes? Presumably, prolonged treatment with an actin poison disrupts not only actin coats but also the preexisting cortical F-actin (i.e., the F-actin associated with the PM). In contrast, a brief treatment (a 4-min cytochalasin D treatment used in this study) is more likely to disrupt only the newly assembling actin coat. Consistent with these assumptions, longer treatment of cytochalasin D also induces collapse of CGs into the PM (data not shown). Thus, these observations suggest that preexisting cortical actin (i.e., actin that is present before exocytosis) provides structural support for the exocytosing CGs, whereas actin coats are essential for compressing exocytosing CGs via barbed end assembly. A compressive role for actin coats is consistent with previous findings: when actin is assembled primarily on one side of the exocytosing CGs, exocytosing CGs are pushed around in the cytoplasm (Yu and Bement, 2007); and when actin coat are uncoupled from the CG membrane upon disruption of myosin-1c function, coat compression is inhibited (Sokac *et al.*, 2006).

In addition to actin assembly, myosin-2 is also involved in compression of the exocytosing compartments. In contrast to the effects of cytochalasin D, inhibition of myosin-2 never completely stalls CG membrane retrieval. In addition, myosin-2 is not recruited to CGs until after the onset of coat compression, implying that myosin-2 does not play a primary role in compressing CG membrane, but in finishing coat compression. How is the recruitment of myosin-2 to actin coats delayed? Because myosin-2 preferentially associates with antiparallel actin filaments, it is possible that earlier in coat assembly, the F-actin that comprises the coats is of insufficient length to permit antiparallel filaments to form.

What role does myosin-1e play? Our results suggest two complementary functions for this motor. First, it seems to be required for complete enclosure of exocytosing CGs by actin coats. In the presence of the headless construct, actin concentrates on the basal side of CG membranes. Curiously, this phenotype is the mirror opposite of that observed after disruption of myosin-1c function, namely, normal initial formation of actin coats near the region of PM-CG fusion, but failure of the coats to track downward over the CG surface to the basal portion (Sokac *et al.*, 2006). Second, myosin-1e may also play a role resisting coat compression until the coat has completely encircled the exocytosing CGs. This is consistent with the ability of cytochalasin to rescue the collapse phenotype in cells expressing headless myosin-1e, and it could help explain why compression does not normally begin until the coats have completely enclosed CGs. This could result if myosin-1e competes with myosin-1c for binding sites on the actin coat to limit the amount of myosin-1c capable of promoting force generation via actin assembly.

Together with previous observations, this study suggests the following model: upon CG-PM fusion, cortical actin structur-

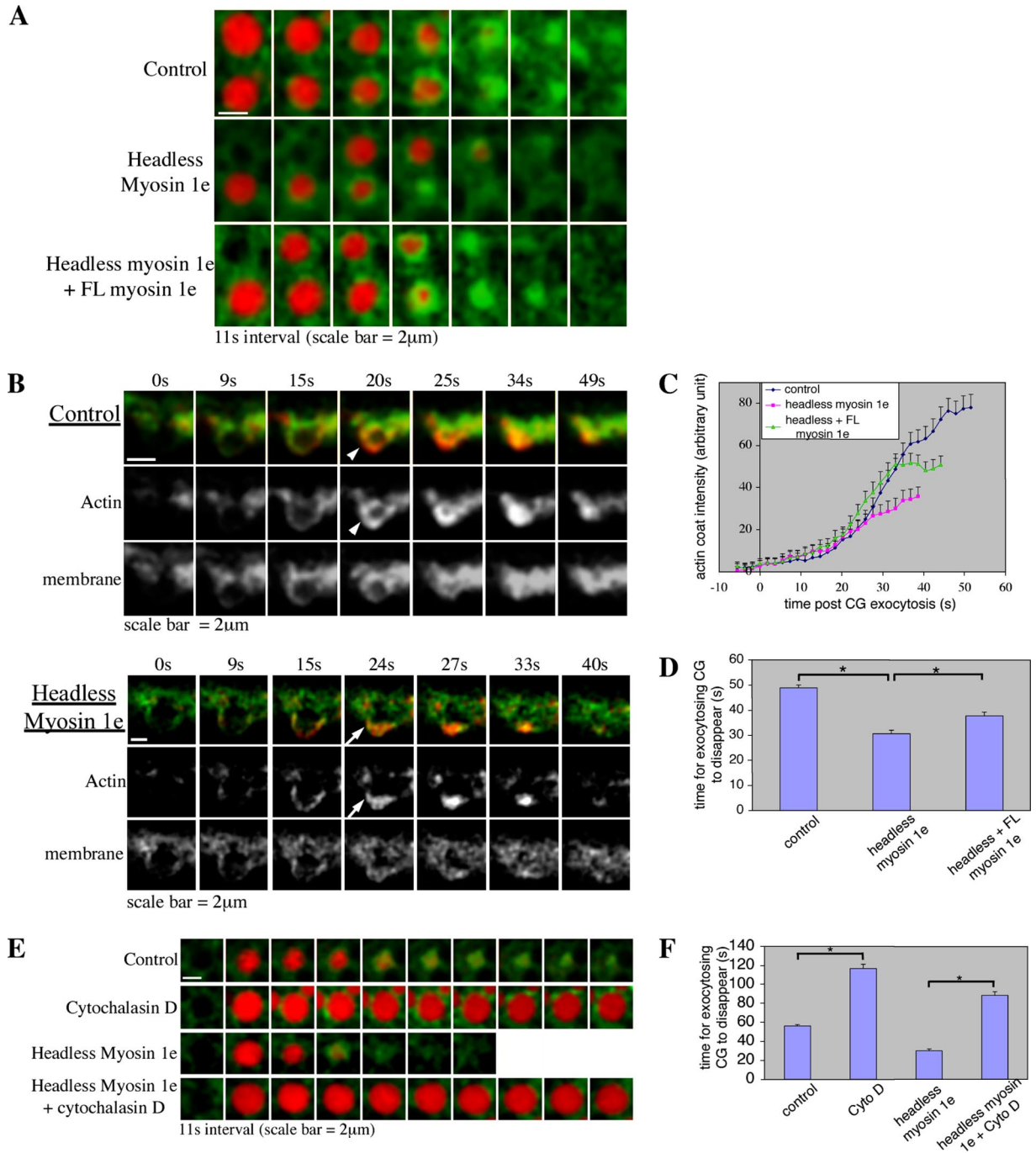


Figure 6. Myosin-1e prevents premature coat compression and ensures symmetric coat assembly. (A) Subcortical images showing expression of the headless myosin-1e leads to faster disappearance of exocytosing CGs (TR-dextran) compare with control. Expression of FL (full-length) myosin-1e in cells expressing the headless myosin-1e rescues the phenotype induced by the headless myosin-1e. The first frame indicates the time at which CGs exocytosed. (B) Z views showing PM (farnesylated-eGFP, green) incorporates into the CG membrane upon CG exocytosis, similar to that illustrated in Yu and Bement (2007). In control cells, the exocytosing CG is subsequently encircled by actin coat (Utr₁₋₂₆₁-mRFP, red, arrowhead). Headless myosin-1e leads to incomplete coat assembly where actin (Utr₁₋₂₆₁-mRFP, red, arrow) is assembled mostly at the basal side of the exocytosing CG (arrow). The first frame indicates the time at which CG exocytosed. (C) Quantification of actin coat intensity, as measured from subcortical images similar to that in A. Actin assembly in cells expressing headless myosin-1e is significantly less than control \sim 30s after CG exocytosis ($p < 0.01$). Coexpression of FL myosin-1e and headless myosin-1e rescues the phenotype. (D) Quantification of time taken for the exocytosing CGs to disappear when imaged subcortically ($n = 80$ for control; $n = 86$ for headless myosin-1e; $n = 70$ for headless myosin-1e with FL myosin-1e; $p = 1 \times 10^{-18}$ for control vs. headless myosin; $p = 0.0005$ for headless myosin-1e vs. coexpression with FL myosin-1e). (E) Subcortical images showing that cytochalasin D treatment in headless myosin-1e-expressing cells results in similar phenotype as cytochalasin D treatment in nonheadless myosin-1e-expressing cells. (F) Quantification of time taken for the exocytosing CGs to disappear when imaged subcortically ($n = 95$ for control; $n = 67$ for cytochalasin D [Cyto D] treated; $n = 79$ for headless myosin-1e; $n = 70$ for headless myosin-1e with cytochalasin D treatment; asterisks represent $p < 5 \times 10^{-6}$). Note that the time shown for cytochalasin D-treated cells (in both normal cells and headless myosin-1e-expressing cells) is an underestimation, because some CGs are still present after the data collection time.

ally supports the exocytosing compartments and prevents their collapse into the PM (Sokac *et al.*, 2003). At the same time, actin assembly begins at the apical side of the CG membrane, and coat compression begins shortly after actin has completely assembled around the entire exocytosing compartments (Sokac *et al.*, 2003). Coat compression is in part provided by plus-end actin assembly (this study). The short-tailed type 1 myosin, myosin-1c, acts to direct assembling actin filament plus ends toward the CG membranes (Sokac *et al.*, 2006). Myosin-1e, a long-tailed myosin-1, ensures both even distribution of coat filaments and that the force produced by the combination of actin assembly and myosin-1c does not result in premature compression of compartments (this study). Later, after the onset of compression, myosin-2 facilitates the final stages of coat closure and membrane retrieval. Thus, at least three myosins are required to facilitate different phases of coat function during CG membrane retrieval.

Finally, the finding that myosin-1e recruitment to the exocytosing CGs depends on its MyTH1 and MyTH2 domains provides a rationale for the recruitment of myosin-1e to CGs. The membrane-binding MyTH1 allows for rapid CG recruitment upon CG-PM fusion, as a result of compartment mixing (Yu and Bement, 2007); the actin-binding MyTH2 allows for further association of myosin-1e with the actin coat, which could be particularly important because myosin-1e functions to prevent premature coat compression. More surprisingly, the results suggest that MyTH2 can preferentially bind to newly assembled actin, which may provide a mechanism by which this class of myosin can be targeted specifically to site where active actin assembly occurs. Although this point remains to be tested definitively, the capacity to bind specifically to newly assembling, highly dynamic actin would provide an additional layer of control of subcellular sorting of myosins-1, in addition to regulation via differential membrane binding (Sokac and Bement, 2000) and regulation via F-actin binding proteins such as tropomyosins (Tang and Ostap, 2001).

ACKNOWLEDGMENTS

We thank B. Burkel for the Utr₁₋₂₆₁ constructs, M. V. Danilchik for the farnesylated-eGFP clone, J. Peloquin for rhodamine myosin-2, and R. Tsien for the mRFP clone. This work is supported by National Institutes of Health grant GM-52932 (to W.M.B.).

REFERENCES

Becker, K. A., and Hart, N. H. (1999). Reorganization of filamentous actin and myosin-II in zebrafish eggs correlates temporally and spatially with cortical granule exocytosis. *J. Cell Sci.* *112*, 97–110.

Benink, H. A., and Bement, W. M. (2005). Concentric zones of active RhoA and Cdc42 around single cell wounds. *J. Cell Biol.* *168*, 429–439.

Bose, A., Guilherme, A., Robida, S. I., Nicoloso, S. M., Zhou, Q. L., Jiang, Z. Y., Pomerleau, D. P., and Czech, M. P. (2002). Glucose transporter recycling in response to insulin is facilitated by myosin Myo1c. *Nature* *420*, 821–824.

Burkel, B. M., von Dassow, G. and Bement, W. M. (2007). Versatile fluorescent probes for actin filaments based on the actin-binding domain of utrophin. *Cell Motil. Cytoskeleton* (*in press*). Epub 8 August 2007.

Doberstein, S. K., and Pollard, T. D. (1992). Localization and specificity of the phospholipid and actin binding sites on the tail of *Acanthamoeba* myosin IC. *J. Cell Biol.* *117*, 1241–1249.

Durrbach, A., Collins, K., Matsudaira, P., Louvard, D., and Coudrier, E. (1996). Brush border myosin-I truncated in the motor domain impairs the distribution and the function of endocytic compartments in an hepatoma cell line. *Proc. Natl. Acad. Sci. USA* *93*, 7053–7058.

Engqvist-Goldstein, A. E., and Drubin, D. G. (2003). Actin assembly and endocytosis: from yeast to mammals. *Annu. Rev. Cell Dev. Biol.* *19*, 287–332.

Jung, G., and Hammer, J. A., 3rd. (1994). The actin binding site in the tail domain of Dictyostelium myosin IC (myoC) resides within the glycine- and proline-rich sequence (tail homology region 2). *FEBS Lett.* *342*, 197–202.

Kaksonen, M., Toret, C. P., and Drubin, D. G. (2005). A modular design for the clathrin- and actin-mediated endocytosis machinery. *Cell* *123*, 305–320.

Kelley, C. A., Sellers, J. R., Gard, D. L., Bui, D., Adelstein, R. S., and Baines, I. C. (1996). *Xenopus* nonmuscle myosin heavy chain isoforms have different subcellular localizations and enzymatic activities. *J. Cell Biol.* *134*, 675–687.

Kimura, K. *et al.* (1996). Regulation of myosin phosphatase by Rho and Rho-associated kinase (Rho-kinase). *Science* *273*, 245–248.

Kolega, J. (1998). Cytoplasmic dynamics of myosin IIA and IIB: spatial ‘sorting’ of isoforms in locomoting cells. *J. Cell Sci.* *111*, 2085–2095.

Kolega, J. (2004). Phototoxicity and photoinactivation of blebbistatin in UV and visible light. *Biochem. Biophys. Res. Commun.* *320*, 1020–1025.

Mandato, C. A., and Bement, W. M. (2001). Contraction and polymerization cooperate to assemble and close actomyosin rings around *Xenopus* oocyte wounds. *J. Cell Biol.* *154*, 785–797.

Mandato, C. A., and Bement, W. M. (2003). Actomyosin transports microtubules and microtubules control actomyosin recruitment during *Xenopus* oocyte wound healing. *Curr. Biol.* *13*, 1096–1105.

Matsumura, F. (2005). Regulation of myosin II during cytokinesis in higher eukaryotes. *Trends Cell Biol.* *15*, 371–377.

May, R. C., and Machesky, L. M. (2001). Phagocytosis and the actin cytoskeleton. *J. Cell Sci.* *114*, 1061–1077.

Merrifield, C. J., Moss, S. E., Ballestrem, C., Imhof, B. A., Giese, G., Wunderlich, I., and Almers, W. (1999). Endocytic vesicles move at the tips of actin tails in cultured mast cells. *Nat. Cell Biol.* *1*, 72–74.

Merrifield, C. J., Qualmann, B., Kessels, M. M., and Almers, W. (2004). Neural Wiskott Aldrich syndrome protein (N-WASP) and the Arp2/3 complex are recruited to sites of clathrin-mediated endocytosis in cultured fibroblasts. *Eur. J. Cell Biol.* *83*, 13–18.

Nemoto, T., Kojima, T., Oshima, A., Bito, H., and Kasai, H. (2004). Stabilization of exocytosis by dynamic F-actin coating of zymogen granules in pancreatic acini. *J. Biol. Chem.* *279*, 37544–37550.

Pelkmans, L., Puntener, D., and Helenius, A. (2002). Local actin polymerization and dynamin recruitment in SV40-induced internalization of caveolae. *Science* *296*, 535–539.

Rogers, S. L., Karcher, R. L., Roland, J. T., Minin, A. A., Steffen, W., and Gelfand, V. I. (1999). Regulation of melanosome movement in the cell cycle by reversible association with myosin V. *J. Cell Biol.* *146*, 1265–1276.

Schietroma, C., Yu, H. Y., Wagner, M. C., Umbach, J. A., Bement, W. M., and Gundersen, C. B. (2007). A role for myosin 1e in cortical granule exocytosis in *Xenopus* oocytes. *J. Biol. Chem.* (*in press*). Epub 16 August 2007.

Sirotkin, V., Beltzner, C. C., Marchand, J. B., and Pollard, T. D. (2005). Interactions of WASp, myosin-I, and verprolin with Arp2/3 complex during actin patch assembly in fission yeast. *J. Cell Biol.* *170*, 637–648.

Sokac, A. M., and Bement, W. M. (2000). Regulation and expression of metazoan unconventional myosins. *Int. Rev. Cytol.* *200*, 197–304.

Sokac, A. M., and Bement, W. M. (2006). Kiss-and-coat and compartment mixing: coupling exocytosis to signal generation and local actin assembly. *Mol. Biol. Cell* *17*, 1495–1502.

Sokac, A. M., Co, C., Taunton, J., and Bement, W. (2003). Cdc42-dependent actin polymerization during compensatory endocytosis in *Xenopus* eggs. *Nat. Cell Biol.* *5*, 727–732.

Sokac, A. M., Schietroma, C., Gundersen, C. B., and Bement, W. M. (2006). Myosin-1c couples assembling actin to membranes to drive compensatory endocytosis. *Dev Cell* *11*, 1–12.

Straight, A. F., Cheung, A., Limouze, J., Chen, I., Westwood, N. J., Sellers, J. R., and Mitchison, T. J. (2003). Dissecting temporal and spatial control of cytokinesis with a myosin II inhibitor. *Science* *299*, 1743–1747.

Sun, Y., Martin, A. C., and Drubin, D. G. (2006). Endocytic internalization in budding yeast requires coordinated actin nucleation and myosin motor activity. *Dev. Cell* *11*, 33–46.

Tang, N., and Ostap, E. M. (2001). Motor domain-dependent localization of myo1b (myr-1). *Curr. Biol.* *11*, 1131–1135.

van Weeren, L., de Graaff, A. M., Jamieson, J. D., Batenburg, J. J., and Valentijn, J. A. (2004). Rab3D and actin reveal distinct lamellar body subpopulations in alveolar epithelial type II cells. *Am. J. Respir. Cell Mol. Biol.* *30*, 288–295.

Verkhovskiy, A. B., Svitkina, T. M., and Borisy, G. G. (1995). Myosin II filament assemblies in the active lamella of fibroblasts: their morphogenesis and role in the formation of actin filament bundles. *J. Cell Biol.* *131*, 989–1002.

Yu, H. E., and Bement, W. M. (2007). Control of local actin assembly by membrane fusion-dependent compartment mixing. *Nat. Cell Biol.* *9*, 149–159.